perpendicular insertion pathway, and two excited states, 1A″ and 2A′, which have a collinear pathway with a 2.3 kcal/mol barrier. The 1A′ and 1A″ surfaces correlate to ground-state products and are not strongly influenced by nonadiabatic interactions (*28*). The 2A′ surface, by contrast, can only react via nonadiabatic coupling. Recently, Gray *et al.* used wave packets and trajectory surface hopping (TSH) calculations (*29*) to demonstrate that reaction can occur on 2A′ at low energies as a result of hopping from 2A′ to 1A′ at long range. In the present work, we have verified that these trajectories give the same product state and angular distributions as those that start on 1A′, and because the 2A′ cross section is small (~6% of 1A′), we have ignored its effect on the product distributions. In contrast, trajectories on the 1A″ surface yield product distributions that are typical for an abstraction reaction: Mostly low rotational states of $v = 3$ and 4 are populated, and backward-scattered angular distributions are seen. The QCT cross section on the 1A″ surface is negligible at 1.3 kcal/mol, but quantum scattering calculations (*29, 30*) find a small cross section due to tunneling that could, in fact, be detectable, especially if the ab initio barrier is slightly too high.

In the QCT results plotted in Figs. 2 to 4, we have included 1A′ results at 1.3 kcal/mol summed with 1A″ results that are based on a slightly higher energy (2.5 kcal/mol) and are multiplied by an empirical scale factor. The scale factor has been adjusted to fit the results for $v = 4$, $N = 4$ in Fig. 2, but this same factor also yields excellent agreement between theory and experiment in Figs. 2 to 4 (only $v = 3$ or 4 are affected by the 1A″ results). The ground-state total cross section is 81.3 atomic units, whereas the scaled 1A″ cross section is 2.6 atomic units. This 1A″ cross section is six times the size estimated from scattering calculations (*30, 31*), but a roughly 0.5 kcal/mol reduction in the barrier would account for the difference. This reduced barrier (1.8 kcal/mol) is also more consistent with that inferred from previous experimental studies (*18, 19*). The QCT results are overall in excellent agreement with experiment, and they demonstrate that most of the observed results are well described using the 1A′ surface. However, the $v = 3$ cross section has a 7% contribution from 1A″, and $v = 4$ has a 35% contribution, and this leads to noticeable backward scattering for these states.

Accurate quantum mechanical calculations on this system are desirable in order to develop a quantitative understanding of this reaction. Our experimental results should be able to provide a test ground for further theoretical studies of this benchmark insertion reaction at the full quantum dynamic level.

### References and Notes

1. Y. T. Lee, *Science* **236**, 793 (1987).
2. L. Schnieder *et al.*, *Science* **269**, 207 (1995).
3. L. Schnieder *et al.*, *J. Chem. Phys.* **107**, 6175 (1997).
4. D. M. Neumark *et al.*, *J. Chem. Phys.* **82**, 3045 (1985).
5. D. M. Neumark *et al.*, *J. Chem. Phys.* **82**, 3067 (1985).
6. M. Faubel *et al.*, *Chem. Phys. Lett.* **232**, 197 (1995).
7. M. Faubel *et al.*, *J. Phys. Chem. A* **102**, 8695 (1998).
8. M. Baer *et al.*, *J. Chem. Phys.* **110**, 10231 (1999).
9. A. L. Ternay Jr., *Contemporary Organic Chemistry* (Sanders, Philadelphia, 1976), pp. 257–260.
10. B. E. Douglas, D. H. MacDaniel, J. J. Alexander, *Concepts and Models of Inorganic Chemistry* (Wiley, New York, ed. 2, 1983), pp. 461–478.
11. G. Anderson, *Annu. Rev. Phys. Chem.* **38**, 489 (1987).
12. G. Dixon-Lewis and D. J. Williams, *Compr. Chem. Kinet.* **17**, 1 (1977).
13. P. Casavecchia, *Rep. Prog. Phys.* **63**, 355 (2000).
14. T. Peng *et al.*, *Chem. Phys. Lett.* **248**, 37 (1996).
15. M. Alagia *et al.*, *J. Chem. Phys.* **108**, 6698 (1998).
16. M. Ahmed, D. S. Peterka, A. G. Suits, *Chem. Phys. Lett.* **310**, 372 (1999).
17. D.-C. Che and K. Liu, *J. Chem. Phys.* **103**, 5164 (1995).
18. Y.-T. Hsu and K. Liu, *J. Chem. Phys.* **107**, 1664 (1997).
19. Y.-T. Hsu, J. H. Wang, K. Liu, *J. Chem. Phys.* **107**, 2351 (1997).
20. Y.-T. Hsu, K. Liu, L. A. Pederson, G. C. Schatz, *J. Chem. Phys.* **111**, 7921 (1999).
21. ———, *J. Chem. Phys.* **111**, 7931 (1999).
22. L. Schnieder *et al.*, *J. Chem. Phys.* **92**, 7027 (1990).
23. Two parallel molecular beams (*para*-$H_2$ and $O_2$) were generated with similar pulsed valves. The $O(^1D)$ atom beam was produced by photolysis of $O_2$ with 157-nm laser light from an $F_2$ laser (Lambda Physik LPX 210I). The $O(^1D)$ beam was then crossed at 90° with the $H_2$ molecular beam. The *para*-$H_2$ molecular beam was generated by expanding the $H_2$ sample through a pulsed nozzle, which was cooled to the liquid nitrogen temperatures (~78 K). The use of a cold nozzle helps reduce the uncertainties of the collisional energy by minimizing the beam velocity spread. A small aperture was used to define the $O(^1D)$ beam between the $O_2$ and $H_2$ beams. The velocity of the $O(^1D)$ beam has been measured to be 2050 m/s with a very narrow velocity distribution ($v/\Delta v > 50$), whereas the velocity of the liquid nitrogen–cooled *para*-$H_2$ beam is 1384 m/s with a speed ratio ($v/\Delta v$) of about 15. [Because *para*-$H_2$ is expanded under the liquid nitrogen temperature, $H_2$ molecules in the beam should be all in the $J = 0$ state (*2, 3*)].
24. J. P. Marangos *et al.*, *J. Opt. Soc. Am. B* **7**, 1254 (1990).
25. During the conversion, detection efficiencies of the H atom product at different LAB angles and different velocities were simulated and thus included in the conversion. For laboratory spectra and product KE distributions for selected angles, see *Science* Online (www.sciencemag.org/feature/data/1052165.shl).
26. D. W. Hwang, X. F. Yang, X. Yang, *J. Chem. Phys.* **110**, 4119 (1999).
27. A. J. Dobbyn and P. J. Knowles, *Faraday Discuss.* **110**, 247 (1998).
28. G. C. Schatz, L. A. Pederson, P. J. Kuntz, *Faraday Discuss.* **108**, 357 (1997).
29. S. K. Gray, C. Petrongolo, K. Drukker, G. C. Schatz, *J. Phys. Chem. A* **103**, 9448 (1999).
30. K. Drukker and G. C. Schatz, *J. Chem. Phys.* **111**, 2451 (1999).
31. S. K. Gray and G. G. Balint-Kurti, personal communication.
32. Supported by NSF grant CHE-9873892 (G.C.S.), the National Science Council and Academia Sinica, and the China Petroleum Company. We thank Y. T. Lee, K. Liu, S. K. Gray, and G. G. Balint-Kurti for insightful discussions.

12 May 2000; accepted 21 June 2000

---

# $^{92}$Nb-$^{92}$Zr and the Early Differentiation History of Planetary Bodies

**C. Münker,[1]* S. Weyer,[1] K. Mezger,[1] M. Rehkämper,[1]
F. Wombacher,[1] A. Bischoff[2]**

**The niobium-92–zirconium-92 ($^{92}$Nb-$^{92}$Zr) extinct radioactive decay system (half-life of about 36 million years) can place new time constraints on early differentiation processes in the silicate portion of planets and meteorites. Zirconium isotope data show that Earth and the oldest lunar crust have the same relative abundances of $^{92}$Zr as chondrites. $^{92}$Zr deficits in calcium-aluminum–rich inclusions from the Allende meteorite constrain the minimum value for the initial $^{92}$Nb/$^{93}$Nb ratio of the solar system to 0.001. The absence of $^{92}$Zr anomalies in terrestrial and lunar samples indicates that large silicate reservoirs on Earth and the moon (such as a magma ocean residue, a depleted mantle, or a crust) formed more than 50 million years after the oldest meteorites formed.**

Current knowledge about geologic and geochemical processes during the early history of Earth is mainly based on isotopic studies of meteorites and old crustal rocks that preserve ages of up to ~4.1 billion years ago (Ga) (*1, 2*). Studies of extinct radioactive decay systems are particularly useful for the study of processes that took place in the early solar system, because they provide better time resolution than long-lived chronometers. Recently, $^{182}$Hf-$^{182}$W chronometry has been used as evidence that the segregation of Earth's core postdates the formation of the solar system by more than 50 million years

---

[1] Zentrallabor für Geochronologie, Mineralogisches Institut, Universität Münster, Corrensstrasse 24, 48149 Münster, Germany. [2] Institut für Planetologie, Universität Münster, Wilhelm Klemm Strasse 10, 48149 Münster, Germany.

*To whom correspondence should be addressed. E-mail: muenker@nwz.uni-muenster.de

(My) (*3*). The search for possible differentiation processes in the early silicate Earth (e.g., early crust formation and mantle depletion) has been confined to the $^{146}$Sm-$^{142}$Nd system (*4–6*), which has a sufficiently long half-life of 106 My. Except for one sample from the Isua Gneiss in Greenland, no measurable $^{142}$Nd/$^{144}$Nd anomaly was detected in Archean rocks (*5, 6*), thus suggesting efficient homogenization of the early silicate Earth or late crust formation. In contrast to Earth, significant $^{142}$Nd/$^{144}$Nd variations have been reported for differentiated meteorites and martian meteorites (*7, 8*). These observations suggest that differences may exist between the timing of differentiation processes in different planetary bodies of the solar system.

A homogeneous early silicate Earth is further supported by Lu-Hf systematics in Archean rocks, in which the initial $^{176}$Hf/$^{177}$Hf ratios scatter tightly around the chondritic value (*9, 10*). However, Hf isotope compositions of many terrestrial rocks appear to be elevated in relation to $^{143}$Nd/$^{144}$Nd (*10, 11*), thus leading to an offset of the terrestrial Hf-Nd array from the chondritic $^{143}$Nd/$^{144}$Nd–$^{176}$Hf/$^{177}$Hf composition. Among other hypotheses, this offset can be explained by the separation of a Mg-perovskite or majoritic garnet residue from Earth's mantle during the possible formation of a Hadean (>4.0 Ga) magma ocean (*11, 12*). Mg-perovskite, the predominant Mg mineral in Earth's deep mantle, has high partition coefficients for Zr and Hf and may thus have caused fractionation of Lu from Hf in the early Earth (*12*).

Here, we report high-precision data for the extinct $^{92}$Nb-$^{92}$Zr nuclide system in terrestrial materials and meteorites. Nb and Zr are lithophile elements and are therefore concentrated in the silicate part of planetary bodies at a chondritic ratio [Nb/Zr = ~0.06 to 0.07 (*13*; this study)]. The isotope $^{92}$Nb decays by electron capture to $^{92}$Zr with a half-life of 36 ± 3 My (*14, 15*). This half-life is about one-third that of the $^{146}$Sm-$^{142}$Nd system. However, the parent-daughter fractionation between major reservoirs of the silicate Earth is an order of magnitude higher for Zr/Nb [~1 to 100 (*13*)] than for Sm/Nd ($^{147}$Sm/$^{144}$Nd = ~0.10 to 0.25). This is because the difference in compatibility between Zr and Nb during clinopyroxene- and garnet-controlled melting is much larger than that between Sm and Nd. Unlike the $^{146}$Sm-$^{142}$Nd chronometer, the $^{92}$Nb-$^{92}$Zr system is also a sensitive tracer for the possible separation of Mg-perovskite from mantle reservoirs in an early magma ocean. Zr is compatible in Mg-perovskite [partition coefficient $K_d$ = 5 to 10 (*12*)], whereas Nb is moderately incompatible [$K_d$ = 0.1 to 1 (*12*)]. Provided that distinct reservoirs formed early in the silicate portion of planets and protoplanets, when $^{92}$Nb was still present, $^{92}$Zr anomalies would be expected if the reservoirs displayed different Zr/Nb ratios. Positive $^{92}$Zr anomalies in relation to chondritic meteorites would be expected for reservoirs with subchondritic Zr/Nb ratios (e.g., a magma ocean or Earth's crust). Conversely, reservoirs that have superchondritic Zr/Nb ratios (e.g., Earth's depleted mantle or a Mg-perovskite residue of a magma ocean) would develop negative $^{92}$Zr anomalies in relation to chondrites. The $^{92}$Zr anomaly is expressed here as

$$\varepsilon^{92}\mathrm{Zr} = \frac{(^{92}\mathrm{Zr}/^{91}\mathrm{Zr})_{\mathrm{sample}} - (^{92}\mathrm{Zr}/^{91}\mathrm{Zr})_{\mathrm{AMES}}}{(^{92}\mathrm{Zr}/^{91}\mathrm{Zr})_{\mathrm{AMES}}} \times 10{,}000 \qquad (1)$$

where "AMES" denotes the $^{92}$Zr/$^{91}$Zr ratio obtained for a standard solution prepared from AMES Zr metal that is used as reference. For a sample that has the same age as the solar system, $^{92}$Zr/$^{91}$Zr is a linear function of Nb/Zr and the initial $^{92}$Nb abundance

$$(^{92}\mathrm{Zr}/^{91}\mathrm{Zr})_{\mathrm{sample}} = (^{92}\mathrm{Zr}/^{91}\mathrm{Zr})_{\mathrm{initial}} + [(^{92}\mathrm{Nb}/^{93}\mathrm{Nb})_{\mathrm{initial}} \times (^{93}\mathrm{Nb}/^{91}\mathrm{Zr})_{\mathrm{sample}}] \qquad (2)$$

where the "initial" Zr and Nb isotope ratios are those at the formation of the solar system. The present-day $^{92}$Zr/$^{91}$Zr and Nb/Zr ratios of meteorites, which formed in the early solar system, are used here to obtain a minimum estimate of the initial $^{92}$Nb/$^{93}$Nb ratio of the solar system. Existing estimates on the initial $^{92}$Nb/$^{93}$Nb ratio, which are based on thermal ionization mass spectrometry (TIMS) or laser-ablation multiple-collector inductively coupled plasma source mass spectrometry (MC-ICPMS) studies on rutiles and zircons in meteorites, range from $1 \times 10^{-3}$ to $2 \times 10^{-5}$ (*16–19*), reflecting the large analytical uncertainty of these methods. In the past, precise measurements of Zr isotopes were hampered by the high first ionization potential of Zr and the isobaric interference of $^{92}$Mo on $^{92}$Zr (*16–18, 20*), thus making Zr unsuitable for analysis by TIMS. The ICP source of MC-ICPMS instruments provides efficient ionization of Zr, and by applying this technique to Zr isotope measurements, it was possible to obtain an external precision of ±0.7 ε units (2σ error) for samples with as little as 50 ng of Zr (*21*).

To evaluate possible variations in the terrestrial Zr isotope composition of different reservoirs, we analyzed zircon grains and whole rock samples of different ages and tectonic settings. Because the oldest known minerals on Earth have an age of ~4.1 Ga (*1, 2*), the preservation of old (>4.1 Ga) silicate reservoirs can only be detected indirectly by the presence of anomalous $^{92}$Zr/$^{91}$Zr ratios in minerals that have inherited the Zr isotope signature of the reservoir from which they were derived. The $^{92}$Zr/$^{91}$Zr ratios of ~30 terrestrial samples (Fig. 1A) agree with the value obtained for the AMES reference solution (*21–23*). Zircons with an age of 3.5 to 4.1 Ga (*1, 24–27*) are among the oldest dated terrestrial minerals and provide representative relics of Earth's early continental crust. Archean mafic rocks [e.g., 3.48-Ga Barberton komatiites and tholeiites, South Africa (*28*)] and xenoliths of Archean lithospheric mantle [e.g., ilmenite xenocryst from the Culinan Kimberlite, South Africa (*29*)] give information on the Zr isotope composition of ancient mantle reservoirs. In contrast to terrestrial zircons and whole rock samples, where only an inherited $^{92}$Nb-$^{92}$Zr signature may have been preserved, Archean Ti-rich minerals (Culinan ilmenite and Mount Narryer rutiles) may provide evidence for live $^{92}$Nb on Earth because of their low Zr/Nb ratio (0.1 to 2) (Fig. 2B). The sample set also includes ~3.3-Ga impact spherules of the Fig Tree Group in South Africa (*30*) to assess the possible contribution of extraterrestrial Zr during the late heavy bombardment of Earth in the early Archean.

The ε$^{92}$Zr values for representative bulk samples of chondrites and eucrites (*31*) agree with the terrestrial values within analytical error; the Zr/Nb ratios scatter around 14. In contrast to the bulk chondrites, some calcium-aluminum–rich inclusions (CAIs) with high Zr/Nb ratios (50 to 70) from the Allende meteorite (*32*) display ε$^{92}$Zr deficiencies of −2 to −4 ε units. The absence of a $^{92}$Zr anomaly in the Allende CAI A-60 (Fig. 2A), which has an anomalously low Zr/Nb ratio (~16), confirms that ε$^{92}$Zr abundances in the CAI are a function of $^{92}$Nb decay. The Allende CAIs represent some of the earliest condensates of the solar nebula and were dated at 4566 ± 2 Ma (*33*). The negative ε$^{92}$Zr values and superchondritic Zr/Nb ratios, which are observed in most Allende CAIs, reflect the selective enrichment of Zr (condensation temperature of ~1800°C) relative to Nb [condensation temperature of ~1600°C at $10^{-3}$ bar (*34*)] during early condensation processes in the solar nebula. Using Eq. 2 and the measured Zr/Nb ratio of the CAI samples (*21*), the initial $^{92}$Nb/$^{93}$Nb ratio of the solar system at 4566 Ma must have been at least 0.001 (Fig. 2A). Such an initial $^{92}$Nb/$^{93}$Nb ratio is sufficient to generate significant $^{92}$Zr/$^{91}$Zr anomalies in typical depleted mantle or crustal reservoirs (Fig. 2B).

ε$^{92}$Zr anomalies in a handpicked clinopyroxene separate of a silicate inclusion in the Caddo County IAB meteorite (*35*) and in a 60-mg split of Adrar 003 (*31*) provide independent evidence for live $^{92}$Nb in the solar system. The negative ε$^{92}$Zr anomaly (−2.2 ± 0.7ε) in the Caddo County meteorite is explained by the high

Zr/Nb ratio (164) in the clinopyroxene, thus suggesting a minimum initial $^{92}$Nb/$^{93}$Nb ratio of 0.0005 (Eq. 2), consistent with $^{147}$Sm-$^{143}$Nd and $^{40}$Ar/$^{39}$Ar ages (*35, 36*) that indicate differentiation and equilibration of Caddo County silicates between ~10 and 50 My after CAI condensation.

$^{92}$Zr/$^{91}$Zr of the two lunar meteorites Dar al Gani 262 and 400, which are fragments of old lunar crust (*37*), overlap with the chondritic and terrestrial $^{92}$Zr/$^{91}$Zr ratios (Fig. 1B). This observation suggests (i) that differentiation of the silicate reservoirs on Earth and the moon is young or (ii) that possible early major silicate reservoirs of the early Earth and the moon were efficiently homogenized after most of the $^{92}$Nb had decayed (Fig. 2A). Because $^{92}$Zr/$^{91}$Zr is identical for Earth and chondrites, Zr isotopes are not suitable for the identification of extraterrestrial impactors of chondritic compositions, such as the Fig Tree Group impact spherules that were shown to originate from a carbonaceous chondrite (*30*). Calculated $\varepsilon^{92}$Zr-Zr/Nb isochrons for 0 to 200 My after the formation of the solar system (Fig. 2B), assuming an initial $^{92}$Nb/$^{93}$Nb ratio of 0.001, indicate that measurable positive $^{92}$Zr anomalies should be preserved in reservoirs with Zr/Nb < 1 (e.g., Ti-rich minerals), even if they crystallized 200

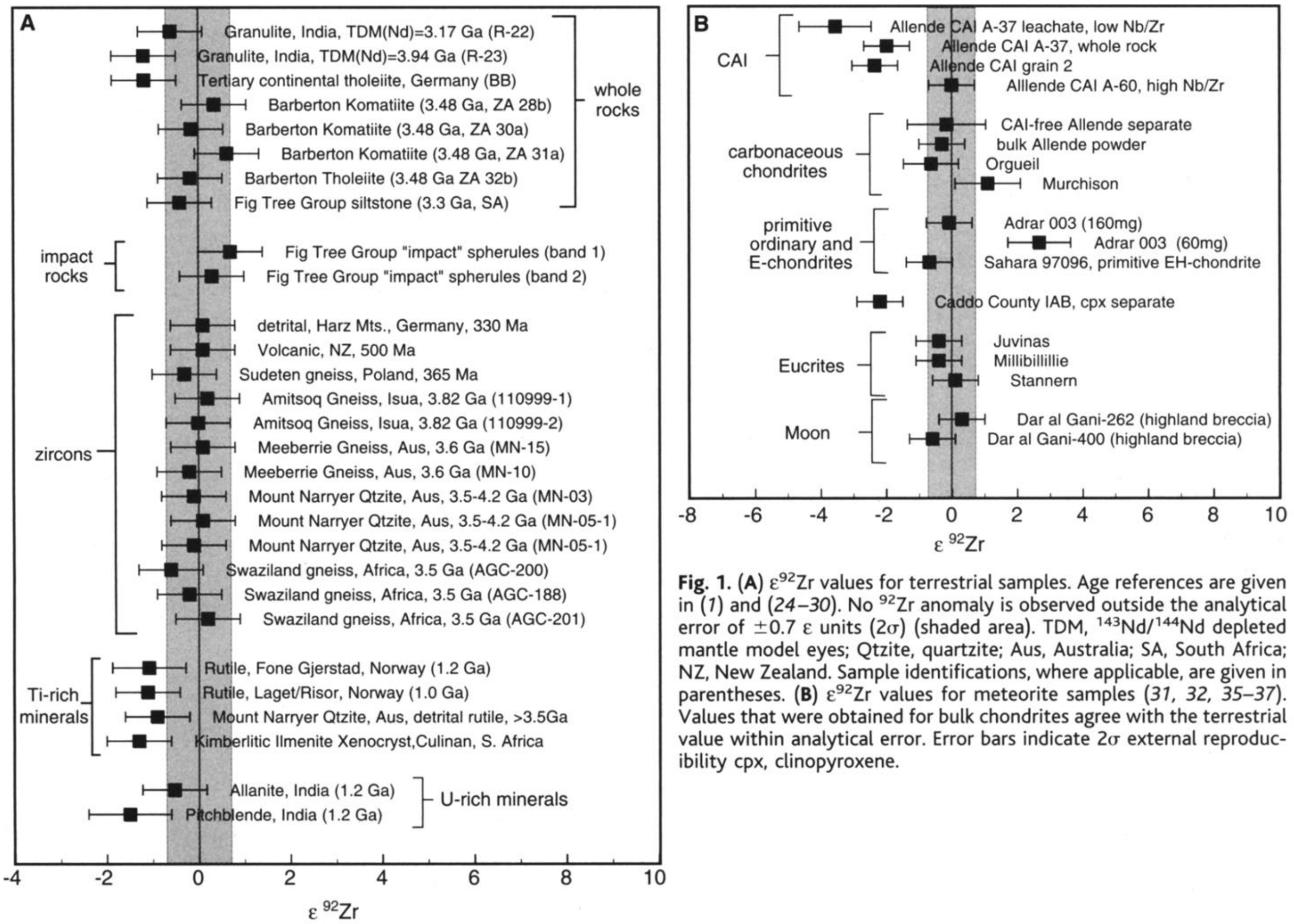

**Fig. 1.** (**A**) $\varepsilon^{92}$Zr values for terrestrial samples. Age references are given in (*1*) and (*24–30*). No $^{92}$Zr anomaly is observed outside the analytical error of ±0.7 ε units (2σ) (shaded area). TDM, $^{143}$Nd/$^{144}$Nd depleted mantle model eyes; Qtzite, quartzite; Aus, Australia; SA, South Africa; NZ, New Zealand. Sample identifications, where applicable, are given in parentheses. (**B**) $\varepsilon^{92}$Zr values for meteorite samples (*31, 32, 35–37*). Values that were obtained for bulk chondrites agree with the terrestrial value within analytical error. Error bars indicate 2σ external reproducibility cpx, clinopyroxene.

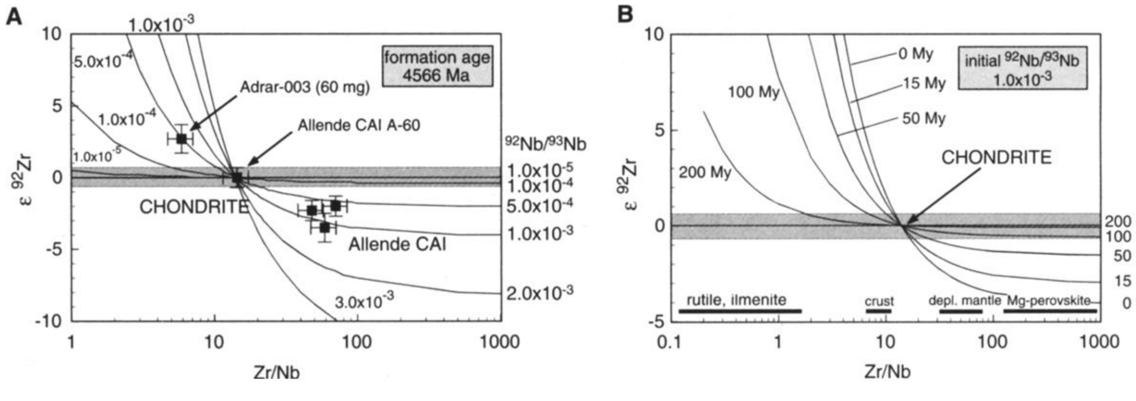

**Fig. 2.** (**A**) $\varepsilon^{92}$Zr versus Zr/Nb isochron diagram for reservoirs that formed at an age of 4.566 Ga (*33*). Allende CAIs fit an isochron suggesting a minimum initial $^{92}$Nb/$^{93}$Nb ratio of ~0.001 for the solar system. Error bars indicate 2σ external reproducibility. (**B**) $\varepsilon^{92}$Zr versus Zr/Nb isochron diagram for formation times of up to 200 My after CAI condensation, assuming an initial $^{92}$Nb/$^{93}$Nb of 0.001. Black bars indicate Zr/Nb ranges of the reservoirs discussed in the text. Shaded areas in (A) and (B) indicate external reproducibility for terrestrial samples.

My after the formation of the solar system. The absence of $^{92}$Zr isotope anomalies in detrital rutiles from Australia and in ilmenite xenocrysts from South Africa (Zr/Nb ratio of 0.1 to 1) therefore indicates that these minerals formed (or equilibrated) later than ~4.3 Ga. A chondritic $\varepsilon^{92}$Zr of the silicate Earth at an initial $^{92}$Nb/$^{93}$Nb ratio of 0.001 implies that the Zr/Nb ratio of Earth lies within ±20% of the chondritic ratio [~14 (this study)] because, otherwise, a resolvable difference in relative $^{92}$Zr abundance as compared to chondrites would be observed (Fig. 2A).

Suggested compositions of Earth's earliest crust include differentiated tonalitic (*38*) and alkaline basaltic lithologies (*39*), similar to lunar KREEP [potassium-, rare-earth element–, and phosphorus-rich basalts]. Remnants of the oldest lunar crust, which date back as far as 4.44 Ga (*40*), include ferroan anorthosites and KREEP (*40, 41*). Depending on the time of formation, such early crust and the corresponding depleted mantle may show $\varepsilon^{92}$Zr values that range up to +2.5 and down to −3, respectively (Figs. 2B and 3). If the crust or depleted mantle formed more than ~50 My after the formation of the solar system, $\varepsilon^{92}$Zr values of these reservoirs would lie within the analytical error of the ratios for chondrites or the present-day bulk silicate Earth (Fig. 3). The uniform $\varepsilon^{92}$Zr values of terrestrial and lunar samples therefore show no vestige of differentiated silicate reservoirs on Earth and the moon that formed within the first 50 My after the birth of the solar system (Fig. 3). The lunar and terrestrial data therefore support constraints from the Sm-Nd (*40*) and Hf-W decay systems (*3*) that date the differentiation of the moon to >50 My after the formation of the solar system, thus supporting an origin of the moon by a collision of a giant impactor with Earth.

A comparison of calculated $\varepsilon^{92}$Zr and $\varepsilon^{142}$Nd for old silicate reservoirs (Fig. 3) reveals that $\varepsilon^{92}$Zr and $\varepsilon^{142}$Nd anomalies would be anticorrelated. This expected anticorrelation is confirmed by combined $\varepsilon^{92}$Zr and $\varepsilon^{142}$Nd (*35*) for clinopyroxene from the Caddo County meteorite (Fig. 3), which has higher Sm/Nd and Zr/Nb ratios than chondrites. A comparison of $^{142}$Nd with $^{92}$Zr abundances therefore enables identification of analytical artifacts. This is particularly useful for old depleted reservoirs, where the expected positive $\varepsilon^{142}$Nd anomalies would be barely resolvable from the chondritic value, given the typical analytical error of TIMS analyses.

The presence of a Hadean magma ocean has been suggested for the early Earth (*42*) and for the moon (*41*). Strong fractionation of Zr from Nb may have occurred during the crystallization of Mg-perovskite in a terrestrial magma ocean (*12*) and during the crystallization of ilmenite and clinopyroxene in a lunar magma ocean (*41*). For Earth, the amount of separated Mg-perovskite is constrained to ~1% because fractionation of additional Mg-perovskite would shift elemental ratios such as Lu/Hf, Hf/Sm, Sc/Sm, or Si/Mg far off the ratios that are presently observed in terrestrial reservoirs (*12*). Nevertheless, the unmixing of only 1% Mg-perovskite would form a reservoir that has high Zr/Nb and high Zr concentrations (resulting in a negative $\varepsilon^{92}$Zr) (Fig. 2B) (*43*). An addition of 10% of such an early perovskite reservoir to a much younger depleted mantle would cause $\varepsilon^{92}$Zr to be less than the silicate Earth value. Likewise, early crystallization of ilmenite (low Zr/Nb) (Fig. 2B) from a lunar magma ocean would have caused negative $^{92}$Zr anomalies in old lunar crust. The absence of significant $\varepsilon^{92}$Zr anomalies in early terrestrial rocks and the early lunar crust therefore argues against the presence of old perovskite and ilmenite reservoirs on Earth and the moon that were created within the first 50 My after the formation of the solar system. The combination of the Zr-Nb system with the Hf-W system (*3*) suggests that the differentiation of Earth and the moon into a metal core and silicate mantle as well as the internal differentiation of this silicate mantle occurred much later than on planetesimals and small planets (e.g., Caddo County IAB meteorite).

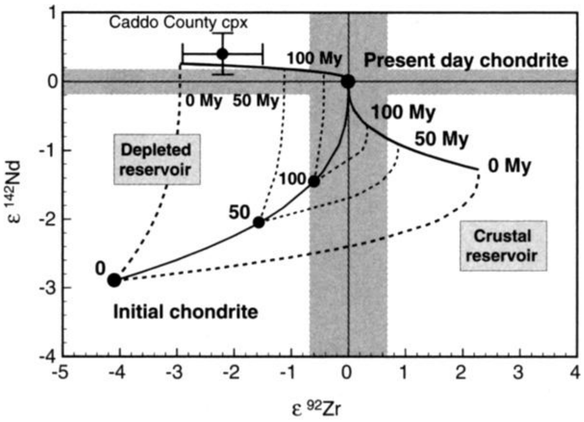

**Fig. 3.** Correlated present-day variations of $\varepsilon^{142}$Nd and $\varepsilon^{92}$Zr that would be expected for old silicate reservoirs in Earth and meteorites (thick solid lines). An initial $^{146}$Sm/$^{144}$Sm value of 0.008 at the condensation time of the solar system is used (*7*) (age corrected to 4566 Ma). $\varepsilon^{142}$Nd-$\varepsilon^{92}$Zr must be anticorrelated because Sm and Zr are more compatible in mantle peridotite than Nd and Nb, respectively. $^{147}$Sm/$^{144}$Nd and Zr/Nb of Earth's depleted mantle [0.214 (*44*) and 50 (*13*), respectively] were assumed for the "depleted" reservoir. For a typical "crustal" reservoir of alkaline basaltic or tonalitic composition, a $^{147}$Sm/$^{144}$Nd value of 0.11 and a Zr/Nb value of 9 were assumed. The chondritic $^{142}$Nd-$^{92}$Zr evolution is shown as a thin solid line; the dashed lines indicate evolution paths for reservoirs that formed 0, 50, and 100 My after the condensation of CAI. The shaded areas indicate typical analytical errors that are reported for TIMS [$^{142}$Nd/$^{144}$Nd (*5, 6*)] and MC-ICPMS [$^{92}$Zr/$^{91}$Zr (this study)].

### References and Notes

1. D. O. Froude, T. R. Ireland, P. D. Kinney, I. S. Williams, W. Compston, *Nature* **304**, 616 (1983).
2. S. A. Bowring, J. E. King, T. B. Housh, C. E. Isachsen, F. A. Podosek, *Nature* **340**, 222 (1989).
3. A. N. Halliday and D. C. Lee, *Geochim. Cosmochim. Acta* **63**, 4157 (1999), and references therein.
4. C. L. Harper and S. B. Jacobsen, *Nature* **360**, 728 (1992).
5. S. L. Goldstein and S. J. G. Galer, *Eos* **73**, 323 (1992).
6. M. T. McCulloch and V. C. Bennett, *Lithos* **30**, 237 (1993).
7. G. W. Lugmair and S. J. G. Galer, *Geochim. Cosmochim. Acta* **56**, 1673 (1992).
8. C. L. Harper Jr., L. E. Nyquist, B. Bansal, H. Wiesmann, C.-Y. Shih, *Science* **267**, 213 (1995).
9. Y. Amelin, D. C. Lee, A. N. Halliday, R. Pidgeon, *Nature* **399**, 252 (1999).
10. J. D. Vervoort and J. Blichert-Toft, *Geochim. Cosmochim. Acta* **63**, 533 (1999).
11. J. Blichert-Toft and N. T. Arndt, *Earth Planet. Sci. Lett.* **171**, 439 (1999), and references therein.
12. T. Kato, E. Ohtani, Y. Ito, K. Onuma, *Phys. Earth Planet. Inter.* **96**, 201 (1996), and references therein.
13. K. P. Jochum, H. M. Seufert, B. Spettel, H. Palme, *Geochim. Cosmochim. Acta* **50**, 1173 (1986).
14. T. Makino and M. Honda, *Geochim. Cosmochim. Acta* **41**, 1521 (1977).
15. D. R. Nethaway, A. L. Prindle, R. A. Van Konyenburg, *Phys. Rev. C* **17**, 1409 (1978).
16. J. F. Minster and C. J. Allègre, *Geochim. Cosmochim. Acta* **46**, 565 (1982).
17. C. L. Harper Jr., *Astrophys. J.* **466**, 437 (1996).
18. S. K. Sahoo and A. Masuda, *Chem. Geol.* **141**, 117 (1997).
19. Q. Z. Yin *et al.*, *Astrophys. J.* **535**, L49 (2000).
20. Mo is a contaminant present in Re filaments that are used for the thermal ionization of Zr with TIMS.
21. Zr isotope measurements were performed with an Isoprobe MC-ICPMS. Except for zircons, Zr and Nb were separated from the whole rock matrix using ion-exchange chromatography. The separation of Zr from Mo was particularly important for samples with high Mo/Zr ratios, such as Ti minerals and chondrites. This is because the $^{92}$Mo interference on $^{92}$Zr can only be corrected adequately if Mo/Zr is <0.005, as tested by repeated measurements of synthetic Mo-Zr mixtures. The Mo/Zr ratios determined for the Zr fractions of the samples that were analyzed in this study were always $<10^{-3}$. The Zr/Nb ratios were determined with an error of ±20% (determined by multiply digested rock standards), using the separated Zr-Nb cut. $^{92}$Zr abundances were analyzed as $^{92}$Zr/$^{91}$Zr and normalized to $^{90}$Zr/$^{91}$Zr = 4.584 [M. Nomura, K. Kogure, M. Okamoto, *Int. J. Mass Spectrum. Ion Phys.* **50**, 219 (1983)], using the exponential law for fractionation correction. An absolute value of $^{92}$Zr/$^{91}$Zr = 1.53120 ± 15 ($2\sigma$; $n$ = 15 averages of measurement sessions) was obtained for the AMES solution over 1 year. Typical external precisions for 10 or more repeated measurements of the AMES Zr metal solution during 1 measurement session were ±0.5 ε units ($2\sigma$) or better at signal intensities of >200 mV for $^{91}$Zr. The external reproducibility for samples was determined with 15 measurements of the zircon sample NZ-159 during 15 different sessions, which gave a value of −0.1 ± 0.7 ε units ($2\sigma$) relative to the AMES Zr standard. This long-term reproducibility of a sample value against the standard value reflects the "true" external reproducibility for samples, rather than the daily within-run reproducibility of the AMES solution. Typical total intensities for Zr were $7 \times 10^{-11}$A per 100 ppb.

Supplemental data are available at www.sciencemag.org/feature/data/1052815.shl.

22. $\varepsilon^{92}$Zr values of the Ti-rich minerals are systematically lower by $\sim$1 $\varepsilon$ unit, although the values are still within the analytical error of the AMES value. This feature is caused by (i) Ti in the Zr fraction (Ti/Zr ratio of $\sim$1 to 5 for Ti minerals) and (ii) the $^{93}$Nb tail on the baseline of $^{92}$Zr. Because Nb was separated together with Zr from the whole rock matrix, this element may cause problems during $^{92}$Zr measurements if Nb/Zr > 1. Such high Nb/Zr ratios were not present in the solutions of other samples.
23. Terrestrial $\varepsilon^{92}$Zr in two 1.2-Ga allanite and pitchblende samples from India, which have high U-Th contents, rules out any substantial $^{92}$Zr contribution from secondary, post-Hadean spallation processes. U-Th–induced $\alpha$-particle irradiation of Nb, Mo, or Y can produce $^{92}$Nb and thus $^{92}$Zr [(*14*); K. E. Apt, J. D. Knight, D. C. Kamp, R. W. Perkins, *Geochim. Cosmochim. Acta* **38**, 1485 (1974)].
24. P. D. Kinney, *Earth Planet. Sci. Lett.* **79**, 337 (1986).
25. A. Kröner, W. Compston, I. S. Williams, *Tectonophysics* **161**, 271 (1989).
26. R. Maas and M. T. McCulloch, *Geochim. Cosmochim. Acta* **55**, 1925 (1991).
27. P. D. Kinney and A. P. Nutman, *Precambrian. Res.* **78**, 165 (1996).
28. M. Lopez-Martinez, D. York, J. A. Hanes, *Precambrian. Res.* **57**, 91 (1992).
29. M. Tredoux, R. J. Hart, R. W. Carlson, S. B. Shirey, *Geology* **27**, 923 (1999).
30. Impact spherules of the lower Fig Tree Group, of which $\sim$50% were supplied from a chondritic impactor, have $^{53}$Cr/$^{52}$Cr values lower than the bulk Earth value, typical of carbonaceous chondrites [A. Shukolyukov, F. T. Kyte, G. W. Lugmair, D. R. Lowe, G. R. Byerly, in *Impacts and the Early Earth*, I. Gilmour and C. Koeberl, Eds. (Springer, Heidelberg, Germany, 2000), vol. 92, pp. 99–116.].
31. The CAI-free Allende sample is a handpicked separate from which visible CAIs were separated. Adrar 003 is an extraordinarily unequilibrated primitive type 3 ordinary chondrite [A. Bischoff, D. W. G. Sears, P. H. Benoit, T. Geiger, T. Stöffler, *LPSCI Contrib.* **XXIII**, 107 (1992)]. A $^{92}$Zr anomaly in a 60-mg split of Adrar 003 confirms that heterogeneities in Zr/Nb are preserved on a mineral but not on a bulk rock scale. Sahara 97096 is a primitive enstatite chondrite [L. Grossman, *Meteorit. Planet. Sci.* **33**, A221 (1998)].
32. The Allende CAI A-37 has been described in detailed by A. Bischoff and H. Palme [*Geochim. Cosmochim. Acta* **51**, 2733 (1987)] and by A. Bischoff, H. Palme, and B. Spettel [*LPSCI Contrib.* **XVIII**, 81 (1987)].
33. C. Göpel, G. Manhès, C. J. Allègre, *Meteoritics* **26**, 338 (1991).
34. A. S. Kornacki and B. Fegley Jr., *Earth Planet. Sci. Lett.* **79**, 217 (1986).
35. B. Stewart, D. A. Papanastassiou, G. J. Wasserburg, *Earth Planet. Sci. Lett.* **143**, 1 (1996).
36. H. Takeda, D. D. Bogard, D. W. Mittlefehldt, D. H. Garrison, *Geochim. Cosmochim. Acta* **64**, 1311 (2000).
37. Dar al Gani 262 and 400 are anorthositic lunar highland breccias [A. Bischoff *et al.*, *Meteorit. Planet. Sci.* **33**, 1243 (1998); J. Zipfel *et al.*, *Meteorit. Planet. Sci.* **33**, A171 (1998)].
38. S. R. Taylor and S. M. McLennan, *Rev. Geophys.* **33**, 241 (1995), and references therein.
39. S. J. G. Galer and S. L. Goldstein, *Geochim. Cosmochim. Acta* **55**, 227 (1991).
40. R. W. Carlson and G. W. Lugmair, *Earth Planet. Sci. Lett.* **90**, 119 (1988).
41. G. A. Snyder, L. A. Taylor, C. R. Neal, *Geochim. Cosmochim. Acta* **56**, 3809 (1992), and references therein.
42. J. Li and C. B. Agee, *Nature* **381**, 686 (1996).
43. Assuming partition coefficient $D_{\mathrm{liq/melt}}$ of 9 for Zr and 0.1 to 1 for Nb in Mg-perovskite (*12*), equilibrium crystallization and the subsequent separation of 1% perovskite from Earth's primitive mantle [$\sim$10 parts per million (ppm) of Zr and 0.6 ppm of Nb] results in a reservoir that has $\sim$80 ppm of Zr and Zr/Nb > 100. Therefore, a Mg-perovskite reservoir would have extremely low $\varepsilon^{92}$Zr (less than –1) if it had formed within the first 50 My after formation of the solar system (Fig. 2A). The addition of $\sim$10% of this reservoir to a younger depleted mantle ($\varepsilon^{92}$Zr = 0, $\sim$6 ppm of Zr) could have generated $\varepsilon^{92}$Zr values that are lower than the silicate Earth value.
44. S. L. Goldstein, R. K. O'Nions, P. J. Hamilton, *Earth Planet. Sci. Lett.* **70**, 221 (1984).

45. This work was supported by grants Me 1717/1-1 and ZG 3/16 of the German Research Council (Deutsche Forschungsgemeinschaft). We thank C. Ballhaus, G. Hanson, E. Scherer, and H. Palme for fruitful discussions. F. Tomaschek, E. Krogstad, K. Rickers, A. Kröner, E. Trapp, M. Bröcker, R. Schumacher, J. Zipfel, and the Barberton Branch of the Geological Society of South Africa generously provided samples or helped during sampling campaigns. Journal reviews by four anonymous referees are appreciated.

9 March 2000; accepted 17 July 2000

---

# A 22,000-Year Record of Monsoonal Precipitation from Northern Chile's Atacama Desert

**J. L. Betancourt,[1]* C. Latorre,[2] J. A. Rech,[3] J. Quade,[3] K. A. Rylander[1]**

**Fossil rodent middens and wetland deposits from the central Atacama Desert (22° to 24°S) indicate increasing summer precipitation, grass cover, and groundwater levels from 16.2 to 10.5 calendar kiloyears before present (ky B.P.). Higher elevation shrubs and summer-flowering grasses expanded downslope across what is now the edge of Absolute Desert, a broad expanse now largely devoid of rainfall and vegetation. Paradoxically, this pluvial period coincided with the summer insolation minimum and reduced adiabatic heating over the central Andes. Summer precipitation over the central Andes and central Atacama may depend on remote teleconnections between seasonal insolation forcing in both hemispheres, the Asian monsoon, and Pacific sea surface temperature gradients. A less pronounced episode of higher groundwater levels in the central Atacama from 8 to 3 ky B.P. conflicts with an extreme lowstand of Lake Titicaca, indicating either different climatic forcing or different response times and sensitivities to climatic change.**

The tropics are believed to be an important source of global climate variability at various time scales, yet their role is poorly understood. Ice age cooling ($\sim$5°C) of the tropics is now evident from many tropical ocean and land records (*1*), raising questions about climate forcing by high versus low latitudes. Precise chronologies of tropical climate change are becoming increasingly necessary to place empirical constraints on competing theories and models. Here, we focus on monsoonal circulation and tropical rainfall over the central Andes. One measure of monsoonal circulation over the central Andes is the variability of summer precipitation (December to March) that spills over from the Altiplano to the Atacama Desert, representing the abrupt, tail end of the tropical rainfall belt.

A history of vegetation change and groundwater fluctuations was reconstructed from $^{14}$C dated fossil rodent middens (*2*) and wetland deposits (*3*) at sites straddling the Tropic of Capricorn (23.5°N) in the central Atacama Desert (Figs. 1 and 2). In the Atacama, several rodents (*Lagidium*, *Phyllotis*, *Abrocoma*, and *Octodontomys*) make urine-hardened cave deposits rich in plant remains akin to North American packrat middens (*2*). Rodent middens afford high taxonomic, spatial, and temporal resolution of past vegetation growing on dry hillslopes and in this study provide important evidence for seasonality of rainfall. Midden records, however, are stratigraphically discontinuous and represent only snapshots of flora through time. In contrast, paleosprings, fed by precipitation in the Andes (>3500 m), have left behind diatomaceous wetland deposits (*3*) that provide a more continuous record of sustained hydrologic changes in the Atacama Desert. The two data sets are strongly complementary and together provide a record of paleoclimatic change that is unprecedented for the region.

Most of the annual precipitation in the Calama and Salar de Atacama basins (Fig. 2) falls in summer but shifts to winter (June to September) only 200 km to the south (Fig. 1). This sharp gradient in seasonality is reflected in southern limits of $\sim$22° to 24°S for most plants that flower in summer versus northern limits of $\sim$25° to 27°S for those that flower in winter (*4*).

---

[1]U.S. Geological Survey, 1675 West Anklam Road, Tucson, AZ 85745, USA. [2]Laboratorio de Botanica, Facultad de Ciencias, Universidad de Chile, Casilla 653, Santiago, Chile. [3]Department of Geosciences, University of Arizona, Tucson, AZ 85721, USA.

*To whom correspondence should be addressed. E-mail: jlbetanc@usgs.gov